Analytical Methods

Accepted Manuscript

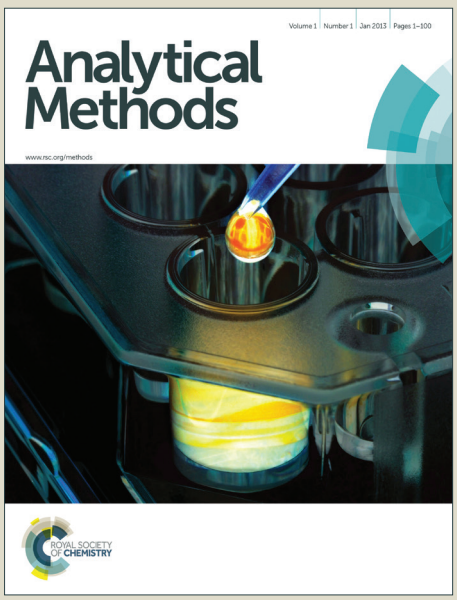

ROYAL SOCIETY OF CHEMISTRY

www.rsc.org/methods

Journal Name

ARTICLE

In-situ preparation of porous Pd nanotubes on GCE for non-enzymatic electrochemical glucose sensor

Received 00th January 20xx,
Accepted 00th January 20xx

DOI: 10.1039/x0xx00000x

www.rsc.org/

Qiang Wang, Qiyu Wang, Kun Qi, Tianyu Xue, Chang Liu, Weitao Zheng and Xiaoqiang Cui*

Porous Pd nanotubes were *in-situ* fabricated on glass-carbon electrode (GCE) via a one-step galvanic replacement reaction by using cheap, flexible, and ultralong copper nanowires as the sacrificial template. The electrode exhibits excellent electrocatalytic performance for non-enzymatic glucose biosensor, thanks to massive pores and high specific surface area. This non-enzymatic glucose biosensor shows a wide linear response range from 5 μM to 10 mM, with a sensitivity of 6.58 μA/mM cm^2, and a detection limit of 1 μM (signal-to-noise ratio of 3).

Introduction

With the increasing incidence of diabetes, it is essential to monitor the blood glucose for the clinical detection and therapy of diabetes.[1] A lot of effective methods have been developed for monitoring of glucose, including enzymatic[2, 3] and non-enzymatic glucose sensors.[4, 5]Recently, more and more attention have been paid for fabricating of non-enzymatic glucose sensors, for avoiding the flaws of enzyme-based sensors, such as insufficient stability, lower reproducibility and oxygen dependence.[6] Various nanomaterials, such as gold,[7, 8] palladium, [9-11] platinum,[12, 13] platinum-lead alloy,[14, 15] cuprous oxide,[16] and gold-lead alloy[17] with controlled shapes and sizes have been explored for the construction of non-enzymatic glucose sensors. Among them, palladium nanostructures have attracted more attention because of their high selectivity, rapid response, and excellent catalytic performances.[10, 18]

The morphology and size are essential to the catalytic properties of palladium nanostructures,[19, 20] which have been extensively investigated in the area of catalysis for CO oxidation,[21] oxygen reduction reaction[22] and formic acid oxidation.[23, 24] For instance, hollow structures with well-defined morphology have shown great enhancement of the catalytic activity due to their high specific surface area, good permeability and high loading capacity.[25-27] The remarkable properties of hollow micro/nanostructures render them greatly promising applications in many areas such as optical sensors,[28] biomedical imaging,[29] catalysis,[30-32] surface-enhanced Raman scattering.[33] Palladium nanotubes (Pd NTs) have shown excellent performances to electrocatalytic reaction of oxygen reduction,[34, 35] ethanol electrooxidation,[36] and hydrogen sensing.[37] Several strategies have been reported for the preparation of Pd NTs, such as, galvanic replacement,[34, 37] chemical deposition,[37, 38] electrodeposition,[39] and molecular adsorption.[40] However, there is still plenty of room remained to seek an environmentally-friendly and simple method for fabricating of Pd NTs with high catalytic activity.

Recently, we found that Pd nanoparticles on graphene nanosheets exhibited excellent catalytic response as a non-enzymatic glucose biosensor.[9] To further improve the performance of glucose sensor, we prepared porous Pd nanotubes on glass-carbon electrode (GCE) by an *in-situ* galvanic replacement strategy using cheap and flexible copper nanowires as sacrificial templates. All reaction process was accomplished under 90 °C Na_2PdCl_4 aqueous solution and the fabrication method is nontoxic and environmentally-friendly. The high specific surface area of this three-dimensional (3D) porous network is beneficial to glucose detection. It is demonstrated that the non-enzymatic glucose sensor constructed by Pd NTs exhibits fast response, wide linear response range, low detection limit, and good selectivity for interfering reagents.

Experimental

Apparatus and reagents

Transmission electron-microscopy (TEM) and high resolution transmission electron microscope (HRTEM) images were obtained by using a JEM-2100F transmission electron microscope (JEOL CO., Japan). Scanning electron microscopy (SEM) images were taken with a JEOL JSM-6700F Field Emission Scanning Electron Microscope. Atomic force

Department of Materials Science, Key Laboratory of Automobile, Materials of MOE and State Key Laboratory of Superhard Materials, Jilin University, Changchun, 130012, People's Republic of China.
E-mail: xqcui@jlu.edu.cn (XQ Cui);
Fax: +86-431-85155279; Tel: +86-431-85155279

microscopy (AFM) images were acquired by using a Bruker Dimension Icon scanning probe microscope (Bruker Co., Germany). X-Ray diffraction (XRD) patterns were collected with the use of a Bragg- Brentano diffractometer (D8-tools, Germany), and the source was a Cu-Kα line at 0.15418 nm. The electrochemical measurements were carried out on a CHI650D electrochemical workstation (Shanghai, Chenhua Co., China). A three-electrode cell was used with a glassy carbon electrode (GCE) as the working electrode, a saturated calomel electrode (SCE) as the reference electrode and a platinum wire electrode as the counter electrode.

Disodium tetrachloropalladate (Na_2PdCl_4), hexadecylamine (HDA, 98%), D-(+)-glucose (99%) were obtained from Sigma-Aldrich. Nafion-ethanol solution was obtained from Adamas-beta Chemical Co (Switzerland). Copper (II) chloride ($CuCl_2{\cdot}2H_2O$, AR), ascorbic acid (AA, AR), uric acid (UA, AR), dopamine (AR), acetamidophenol (AR) were purchased from Beijing chemical works, China. Sodium hydroxide (NaOH, AR), n-hexane (AR), and ethanol (AR) were purchased from Sinopharm Chemical Reagent, China. Deionized water was used throughout the experiments.

Synthesis of Cu nanowires modified GCE

Cu nanowires (NWs) were prepared according to previous report with slight modification.[41] In a typical synthesis, $CuCl_2{\cdot}2H_2O$ (21 mg), glucose (50 mg), HDA (180 mg), deionized water (10 mL) were mixed in a glass vial, with stirring for 6 hour to obtain light-blue emulsion. The capped vial was transferred into an oil bath and heated at 100 °C for 6 h to obtain a reddish-brown solution. The Cu NWs were purified by centrifuging the reddish-brown solution at 2000 rpm for 10 min. The precipitation was washed with n-hexane, ethanol and water (60 °C) sequentially. Finally, the product was dispersed into deionized water (0.5 mL) with ultrasonic for 10 min, 8 µL of as-prepared Cu nanowires suspension was dropped onto a GCE surface (GCE, 3 mm in diameter) and dried under vacuum for 4 h at room temperature.

***In-situ* synthesis of Pd nanotubes on GCE**

5 mL of 68 mM Na_2PdCl_4 solution was saturated by nitrogen gas for 15 min in a glass beaker (10 mL), the beaker was transferred into a water bath and kept at 90 °C for 10 min without stirring. The as-prepared Cu NWs modified GCE was placed into the Na_2PdCl_4 solution for another 30 min, and subsequently dried under vacuum condition for 2 h at room temperature. 5 µL of Nafion (0.5%) was used to cover the surface of the electrode. All electrochemical characterizations were accomplished in solutions with nitrogen saturation.

Results and discussion

Preparation and characterization of Cu NWs and Pd NTs

Cu nanowires were synthesized according to previous report with slight modification[41] and assembled on GCE to form 3D network. The Pd nanotubes were then *in-situ* fabricated on GCE via a one-step galvanic replacement reaction by using these copper nanowires as the sacrificial template in Na_2PdCl_4 aqueous solution. Scheme 1 shows the overall procedure for the preparation of porous palladium nanotubes with high surface area/volume ratio on the GCE.

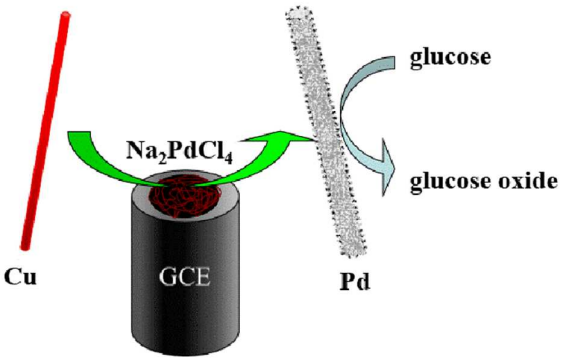

Scheme 1 Fabrication of Pd NTs on GCE for non-enzymatic glucose sensor.

As-prepared Cu NWs assembled on GCE were characterized by SEM, TEM and AFM as shown in Fig. 1(A)-(C). SEM image (Fig. 1A) shows that the assembled Cu NWs exhibit 3D network on GCE, and the diameters are calculated to be of 61 ± 6 nm with the length of several micrometers. TEM image (Fig.1B) confirms that ultralong, solid internal Cu NWs have been successfully prepared. The high-resolution TEM (HRTEM) image (Fig. 1B, inset) shows that the lattice spacing is of 2.1 Å, which corresponds to the lattice spacing of Cu. AFM is another efficient technique to present the morphology of the product. As shown in Fig. 1C, the height of Cu NWs obtained from the 3D image of AFM is about 60 nm with the length of several micrometers, which is consistent with SEM and TEM results. After one-step galvanic replacement reaction, morphological

change of the nanostructures were monitored by SEM, TEM and

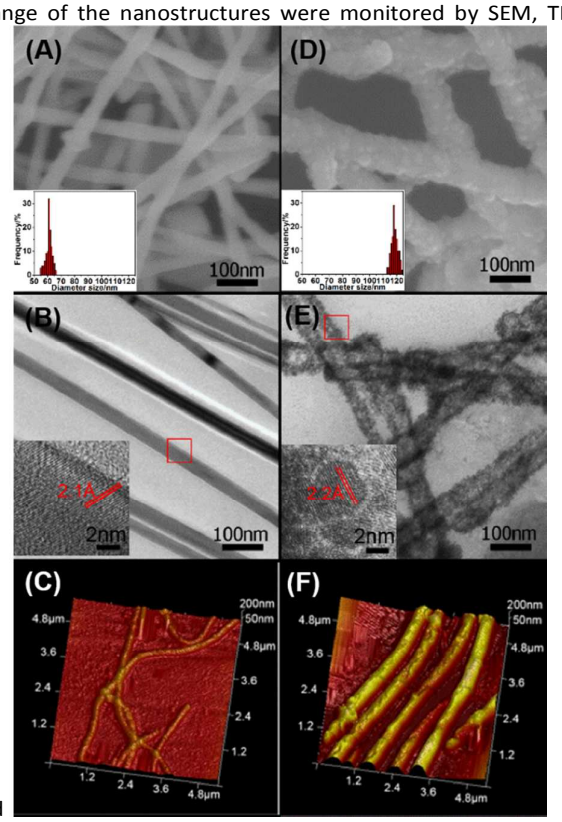

Fig.1 SEM, TEM images and AFM topography images of Cu NWs (A, B, C) and Pd NTs (D, E, F), the insets are the distribution of diameters, HRTEM images of Cu NWs and Pd NTs.

AFM, as shown in Fig. 1(D)-(F). SEM image (Fig. 1D) shows that the diameters of the produces are increased to 118 ± 6 nm while keeping the 3D network structure of copper NWs. The nanostructures shown in the TEM image (Fig.1E) seem to be nearly transparent suggesting that they have hollow interiors, indicating that Pd NTs were obtained. High-resolution TEM (HRTEM) image (Fig. 1E, inset) shows the lattice spacing is of 2.2 Å that is correspond to the lattice spacing of Pd. The inset in Fig. 1(E) also reveals that Pd NTs are composed of highly rough shells that are formed by the aggregation of small Pd nanograins. The height of Pd NTs obtained from the 3D image of AFM (Fig.1F) is also increased from 60 nm to 115 nm.

X-ray diffraction (XRD) patterns are shown in Figure 2 to confirm the crystalline structure of the obtained products. XRD pattern of Cu NWs (JCPDS #03-1018) shows well-defined peaks at 2Θ = 43.5, 50.7, 74.7, and 90.1° correspond to the {111}, {200}, {220}, and {311} planes for a face-centered-cubic (fcc) structure. The planes of Cu_2O or CuO were not detected. Pd (JCPDS #46-1043) peaks at 2Θ = 40.1, 46.7, 68.1, 82.1, and 86.6° correspond to the {111}, {200}, {220}, {311}, and {222} planes for a face-centered cubic (fcc) structure. No observable diffraction peaks of CuPd alloy appeared indicates the copper has been completely consumed and the single-phase Pd NTs have been formed.

Electrochemical characterization of Pd NTs/GCE

The electrochemical behavior of Pd NTs was investigated by cyclic voltammograms in N_2-saturated 0.1 M NaOH solution. As shown in Fig. 3(A), the anodic peak at -0.1 V was ascribed to the formation of Pd-OH and the rapidly increased current at 0.6 V was corresponding to Pd oxidation. In negative scan, the cathodic peak at 0.1 V was related to the reduction of Pd oxide.[10, 18] The anodic or cathodic peak currents increase linearly with scan rates from 20 to 140 mV/s (Fig. 3(B)), indicating that the electrochemical reaction is a surface-controlled process.[18, 42]

The electrochemical catalytic property of as-prepared Pd NTs was investigated by measuring the CV response in N_2-saturated 0.1 M NaOH aqueous solution as shown in Fig. 4(A). In presence of glucose, two anodic peaks are observed at-0.15 V and 0.48 V during positive scan. Current peak at -0.15 V should be ascribed to the electro-absorption of glucose to form

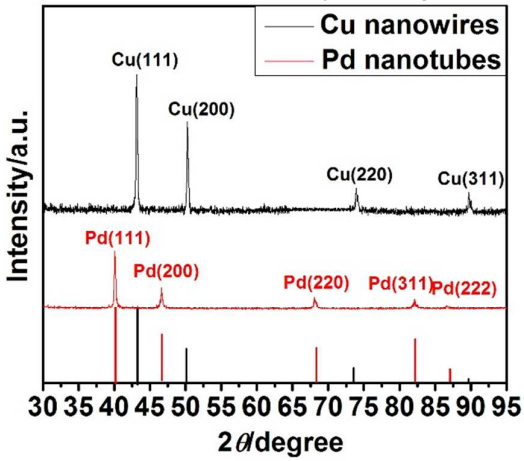

Fig.2 XRD patterns of the Cu NWs and Pd NTs.

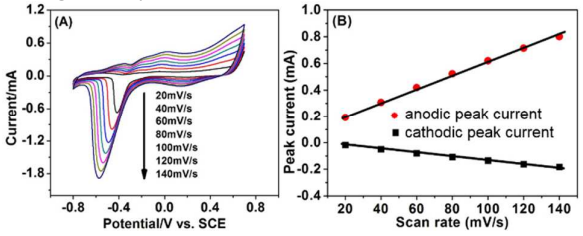

Fig.3 (A) Cyclic voltammograms of Pd NTs/GCE in 0.1 M NaOH solution at different scan rates (from 20 to 140 mV/s). (B) Plots of peak currents versus scan rates.

intermediate during which per glucose molecule loses one proton in this electrochemical reaction.[10] Pd-OH species are generated in the alkaline solution when the applied potential was higher than 0.20 V, which is beneficial to oxidation of the intermediates from the glucose electroadsorption.[10] The second current peak at 0.48 V derives from consequent oxidation of the intermediate on Pd NTs surfaces. Decrease of the current at the higher applied potential could be due to the formation of Pd oxide that covered the active sites on Pd surfaces. During the negative scan, the single cathodic peak at -0.35 V was related to the reduction of Pd oxide. In the range of +0.70 V to -0.20 V, glucose could not be oxidized due to the oxidation of Pd surfaces. As the continuing negative scan, the oxidized Pd surfaces were reduced and surface-active sites were renewed, resulting in a new electrocatalytic peak at -0.39

V. Fig. 4(B) depicts CVs of bare GCE, Cu NW s/GCE and Pd NTs/GCE in the presence of 5 mM glucose. From the CV curves, bare GCE and Cu NWs/GCE show unobservable response to glucose, comparing with the remarkable oxidation signal of glucose of the Pd NTs/GCE at about 0.48 V. It demonstrates that the as-prepared Pd hollow nanotubes present high catalytic activity to the oxidation of glucose in alkaline solution.

Amperometric sensing of glucose

The sensor was evaluated by amperometric measurement in N_2-saturated 0.1 M NaOH aqueous solution by successive step-wise additions of glucose as shown in Fig. 5(A). Pd NTs/GCE showed a remarkable and sensitive response to the changes of glucose concentration (5 μM ~10 mM), which could be ascribed to the porous surface structure of 3D network. As shown in Fig. 5(B), the amperometric response is linearly correlated with glucose concentration in the range of 5 μM ~10 mM, with a detection limit of 1 μM (signal-to-noise ratio of 3).Table1 shows a comparison of the sensitivity and linear range between Pd NTs and other Pd (or Pt) nanomaterials used for non-enzymatic glucose sensing. Porous Pd NTs in this work shows the best detection limit and linear range. The response current remains at 80% after two weeks storage in the refrigerator.

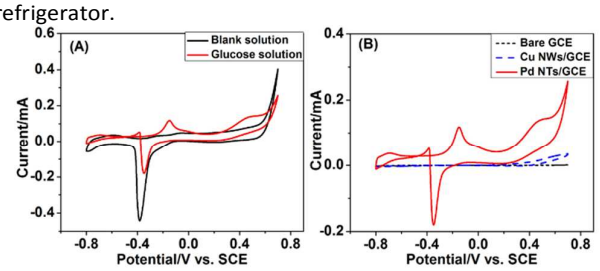

Fig.4 (A) CVs of Pd NTs/GCE with and without 5 mM glucose in 0.1 M NaOH at a scan of 10 mVs^{-1}. (B) CVs of bare GCE, Cu NWs/GCE and Pd NTs/GCE in presence of 5 mM glucose.

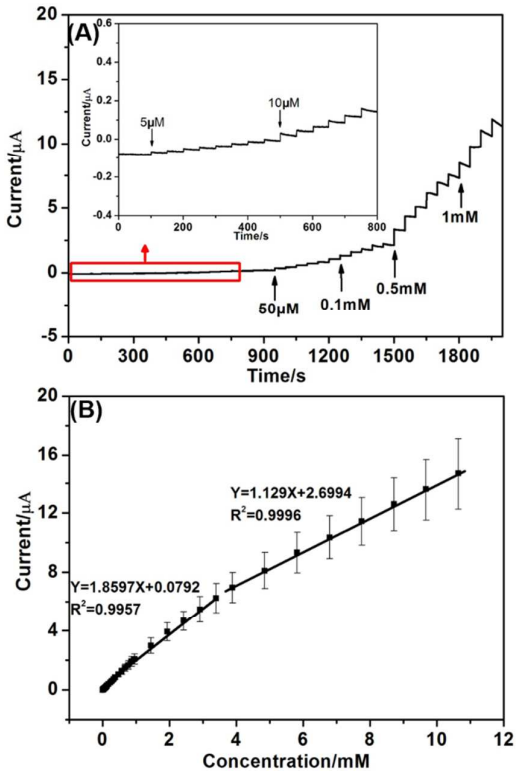

Fig.5 (A) Amperometric response of the Pd NTs/GCE to the successive addition of glucose into 0.1 M NaOH solution at 0.4 V, inset is the enlarged response from red rectangle marked area. (B) The linear relationship between the response current and the glucose concentration is shown.

Table 1

Comparison of the sensitivity and linear range between porous Pd NTs and other Pd (Pt) materials for non-enzymatic glucose sensing.

Electrode	Sensitivity ($\mu AmM^{-1}cm^{-2}$)	Linear range (mM)	Ref.
Porous Pd NTs	6.58	0.005-10	this work
Pd NPs/graphene oxide	Not given	0.2-10	9
Pd nanocubes	34	1-10	43
Pd NPs/graphene	Not given	0.01-5	18
Pt NPs/multi-walled carbon nanotubes	11.83	1-8	44
Pt NPs/ multi-walled carbon nanotubes	106	0-2.4	45
Pt NPs/mesoporous carbon	8.53	0.005-7.5	46

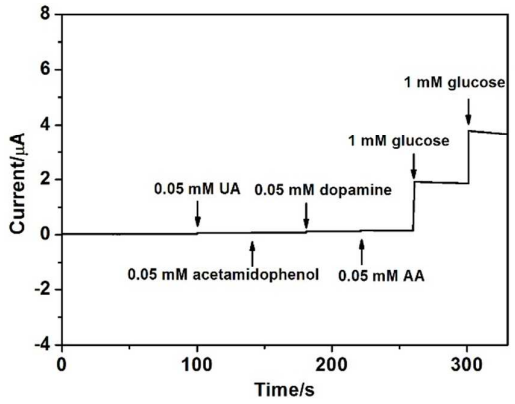

Fig.6 Typical current–time dynamic response of Pd NTs/GCE towards interferences and glucose in NaOH (0.1 M) at 0.4 V.

Table 2

Interferences response to glucose detection at 0.4 V.

Substrate	Concentration (mM)	Response current (μA)
Glucose	1	1.87
Ascorbic acid	0.05	0.037
Uric acid	0.05	0.044
Dopamine	0.05	0.042
Acetamidophenol	0.05	0.018

Interferences

The ability to discriminate common electroactive interferences is an important factor for glucose sensor since the electron transfer rates of these interferences are relatively faster than glucose when they are oxidized.[10, 11] Typical current density–time dynamic response of as- synthesized Pd NTs/GCE towards interferences (0.05 mM AA, 0.05 mM UA, 0.05 mM dopamine, 0.05 mM acetamidophenol) and glucose in NaOH (0.1 M) at 0.4 V is shown in Fig.6. The results summarized in Table 2 indicate that the responses from AA, UA, dopamine and acetamidophenol are negligible compared to the electrochemical detection of glucose.

Real sample analysis

Pd NTs/GCE was also used to detect the concentration of glucose in human blood serum samples. The recovery of glucose was determined by standard addition of pure glucose to the serum samples and the corresponding results are shown in Table 3. The results shows that the proposed sensor gives good recoveries. The potential interfering species in serum do not affect the glucose detection.

Conclusions

In conclusion, we have demonstrated a simple and facial approach to *in-situ* synthesis of Pd NTs on GCE via a one-step galvanic replacement reaction by using cheap and flexible copper nanowires as the sacrificial template. All reaction process was accomplished under 90 °C aqueous solution and the fabrication method is nontoxic and environmentally-friendly. The 3D porous network and high specific surface area of Pd NTs are beneficial to glucose detection. XRD, TEM and HRTEM were employed to characterize the structure and composition of as-obtained Pd nanostructure. The Pd NTs we prepared on GCE exhibited excellent electrocatalytic performance as a non-enzyme glucose biosensor in alkaline solution. This glucose biosensor shows a wide linear response range from 5 μM to 10 mM, with a detection limit of 1 μM (signal-to-noise ratio of 3) at a detection potential of 0.4 V.

Table 3

Determination of glucose in blood serum samples at 0.4 V.

Sample	Diluted (mM)	Add (mM)	Found (mM)	Recovery (%)
1	0.84	5	5.75	98.3
2	1.37	5	6.29	98.4
3	1.58	5	6.54	99.2

Acknowledgements

This work was financially supported by the National Natural Science Foundation of China (No. 21275064, 21075051), Program for New Century Excellent Talents in University (NCET-10-0433), Specialized Research Fund for the Doctoral Program of Higher Education (20130061110035).

Notes and references

1 K. J. Cash and H. A. Clark, *Trends. Mol. Med.*, 2010, **16**, 584-593.
2 Q. Liu, X. B. Lu, J. Li, X. Yao and J. H. Li, *Biosens. Bioelectron.*, 2007, **22**, 3203-9.
3 S. Z. Bas, *Anal. Methods*, 2014, **6**, 7752-7759.
4 H. Gao, F. Xiao, C. B. Ching and H. Duan, *ACS Appl Mater Interfaces*, 2011, **3**, 3049-57.
5 C. Guo, H. Huo, X. Han, C. Xu and H. Li, *Anal. Chem.*, 2014, **86**, 876-83.
6 G. F. Wang, X. P. He, L. L. Wang, A. X. Gu, Y. Huang, B. Fang, B. Y. Geng and X. J. Zhang, *Microchim. Acta*, 2013, **180**, 161-186.
7 Y. Bai, W. W. Yang, Y. G. Sun and C. Q. Sun, *Sensor. Actuat. B-Chem.*, 2008, **134**, 471-476.
8 Y. Zhao, J. Chu, S. H. Li, W. W. Li, G. Liu, Y. C. Tian and H. Q. Yu, *Electroanal.*, 2014, **26**, 656-663.
9 Q. Y. Wang, X. Q. Cui, J. L. Chen, X. L. Zheng, C. Liu, T. Y. Xue, H. T. Wang, Z. Jin, L. Qiao and W. T. Zheng, *Rsc. Adv.*, 2012, **2**, 6245-6249.
10 X. M. Chen, Z. J. Lin, D. J. Chen, T. T. Jia, Z. M. Cai, X. R. Wang, X. Chen, G. N. Chen and M. Oyama, *Biosens. Bioelectron.*, 2010, **25**, 1803-1808.
11 L. Meng, J. Jin, G. Yang, T. H. Lu, H. Zhang and C. X. Cai, *Anal. Chem.*, 2009, **81**, 7271-7280.
12 H. Tang, J. H. Chen, S. Z. Yao, L. H. Nie, G. H. Deng and Y. F. Kuang, *Anal. Biochem.*, 2004, **331**, 89-97.
13 L. Q. Rong, C. Yang, Q. Y. Qian and X. H. Xia, *Talanta*, 2007, **72**, 819-824.
14 Y. Bai, Y. Y. Sun and C. Q. Sun, *Biosens. Bioelectron.*, 2008, **24**, 579-585.

15 M. F. Hossain and J. Y. Park, *Electroanal.*, 2014, **26**, 940-951.
16 M. M. Liu, R. Liu and W. Chen, *Biosens. Bioelectron.*, 2013, **45**, 206-12.
17 M. Tominaga, T. Shimazoe, M. Nagashima, H. Kusuda, A. Kubo, Y. Kuwahara and I. Taniguchi, *J. Electroanal. Chem.*, 2006, **590**, 37-46.
18 L. M. Lu, H. B. Li, F. L. Qu, X. B. Zhang, G. L. Shen and R. Q. Yu, *Biosens. Bioelectron.*, 2011, **26**, 3500-3504.
19 Y. Zhang, P. L. Zhu, L. Chen, G. Li, F. R. Zhou, D. Q. Lu, R. Sun, F. Zhou and C. P. Wong, *J. Mater. Chem. A*, 2014, **2**, 11966-11973.
20 L. Zhang, W. Niu and G. Xu, *Nanoscale*, 2011, **3**, 678-82.
21 Z. N. Xu, J. Sun, C. S. Lin, X. M. Jiang, Q. S. Chen, S. Y. Peng, M. S. Wang and G. C. Guo, *ACS Catal.*, 2013, **3**, 118-122.
22 L. Xiao, L. Zhuang, Y. Liu, J. T. Lu and H. D. Abruna, *J. Am. Chem. Soc.*, 2009, **131**, 602-608.
23 X. X. Wang, J. D. Yang, H. J. Yin, R. Song and Z. Y. Tang, *Adv. Mater.*, 2013, **25**, 2728-2732.
24 H. Zhao, J. Yang, L. Wang, C. G. Tian, B. J. Jiang and H. G. Fu, *Chem. Commun.*, 2011, **47**, 2014-2016.
25 S. C. Yang and X. Luo, *Nanoscale*, 2014, **6**, 4438-4457.
26 X. H. Xia, Y. Wang, A. Ruditskiy and Y. N. Xia, *Adv. Mater.*, 2013, **25**, 6313-6333.
27 K. Qi, Q. Y. Wang, W. T. Zheng, W. Zhang and X. Q. Cui, *Nanoscale*, 2014, **6**, 15090-7.
28 Y. G. Sun and Y. N. Xia, *Anal. Chem.*, 2002, **74**, 5297-5305.
29 J. Y. Chen, B. Wiley, Z. Y. Li, D. Campbell, F. Saeki, H. Cang, L. Au, J. Lee, X. D. Li and Y. N. Xia, *Adv. Mater.*, 2005, **17**, 2255-2261.
30 H. H. Li, C. H. Cui, S. Zhao, H. B. Yao, M. R. Gao, F. J. Fan and S. H. Yu, *Adv. Energy. Mater.*, 2012, **2**, 1182-1187.
31 S. W. Kim, M. Kim, W. Y. Lee and T. Hyeon, *J. Am. Chem. Soc.*, 2002, **124**, 7642-7643.
32 G. D. Nie, X. F. Lu, J. Y. Lei, L. Yang, X. J. Bian, Y. Tong and C. Wang, *Electrochim. Acta*, 2013, **99**, 145-151.
33 Z. Y. Jiang, Q. F. Zhang, C. Zong, B. J. Liu, B. Ren, Z. X. Xie and L. S. Zheng, *J. Mater. Chem.*, 2012, **22**, 18192-18197.
34 S. M. Alia, K. Duong, T. Liu, K. Jensen and Y. Yan, *ChemSusChem*, 2014, **7**, 1739-44.
35 M. Mohl, D. Dobo, A. Kukovecz, Z. Konya, K. Kordas, J. Q. Wei, R. Vajtai and P. M. Ajayan, *J. Phys. Chem. C*, 2011, **115**, 9403-9409.
36 A. L. Wang, H. Xu, J. X. Feng, L. X. Ding, Y. X. Tong and G. R. Li, *J. Am. Chem. Soc.*, 2013, **135**, 10703-9.
37 S. F. Yu, U. Welp, L. Z. Hua, A. Rydh, W. K. Kwok and H. H. Wang, *Chem. Mater.*, 2005, **17**, 3445-3450.
38 S. Z. Chu, H. Kawamura and M. Mori, *J. Electrochem. Soc.*, 2008, **155**, D414.
39 S. Cherevko, J. Fu, N. Kulyk, S. M. Cho, S. Haam and C. H. Chung, *J. Nanosci.Techno.*, 2009, **9**, 3154-3159.
40 M. Steinhart, Z. H. Jia, A. K. Schaper, R. B. Wehrspohn, U. Gosele and J. H. Wendorff, *Adv. Mater.*, 2003, **15**, 706-709.
41 M. S. Jin, G. N. He, H. Zhang, J. Zeng, Z. X. Xie and Y. N. Xia, *Angew. Chem. Int. Ed.*, 2011, **50**, 10560-10564.
42 S. J. Bao, C. M. Li, J. F. Zang, X. Q. Cui, Y. Qiao and J. Guo, *Adv. Funct. Mater.*, 2008, **18**, 591-599.
43 J. S. Ye, C. W. Chen and C. L. Lee, *Sensor. Actuat. B-Chem.*, 2015, **208**, 569-574.
44 L.-H. Li and W.-D. Zhang, *Microchim. Acta*, 2008, **163**, 305-311.
45 H.-W. Chang, Y.-C. Tsai, C.-W. Cheng, C.-Y. Lin and P.-H. Wu, *Sensor. Actuat. B-Chem.*, 2013, **183**, 34-39.
46 C. Su, C. Zhang, G. Lu and C. Ma, *Electroanal.*, 2010, **22**, 1901-1905.